



HAL
open science

Simulation of motor unit action potential recordings from intramuscular multichannel scanning electrodes

Konstantin Akhmadeev, Tianyi Yu, Éric Le Carpentier, Yannick Aoustin, Dario Farina

► **To cite this version:**

Konstantin Akhmadeev, Tianyi Yu, Éric Le Carpentier, Yannick Aoustin, Dario Farina. Simulation of motor unit action potential recordings from intramuscular multichannel scanning electrodes. *IEEE Transactions on Biomedical Engineering*, 2020, 67 (7), pp.2005-2014. 10.1109/TBME.2019.2953680 . hal-02362499

HAL Id: hal-02362499

<https://hal.science/hal-02362499v1>

Submitted on 13 Nov 2019

HAL is a multi-disciplinary open access archive for the deposit and dissemination of scientific research documents, whether they are published or not. The documents may come from teaching and research institutions in France or abroad, or from public or private research centers.

L'archive ouverte pluridisciplinaire **HAL**, est destinée au dépôt et à la diffusion de documents scientifiques de niveau recherche, publiés ou non, émanant des établissements d'enseignement et de recherche français ou étrangers, des laboratoires publics ou privés.

Simulation of motor unit action potential recordings from intramuscular multichannel scanning electrodes

Akhmadeev Konstantin, Tianyi Yu, Eric Le Carpentier, Yannick Aoustin, Dario Farina, *Fellow, IEEE*

Abstract—Multichannel intramuscular EMG (iEMG) recordings provide information on motor neuron behaviour, muscle fiber (MF) innervation geometry and, recently, have been proposed as means for establishing human-machine interfaces. **Objective:** in order to provide a reliable benchmark for computational methods applied to such recordings, we propose a simulation model for iEMG signals acquired by intramuscular multi-channel electrodes. **Methods:** we propose a number of modifications to the existing iEMG simulation methods, such as farthest point sampling for more uniform motor unit innervation centers distribution in the muscle cross-section, fiber-neuron assignment algorithm, motor neuron action potential propagation delay modelling and a linear model for multichannel recordings simulation. The proposed approach is also extended to gradually shifting (scanning) electrodes. **Results:** we provide representative applications of this model to the validation of methods for the estimation of motor unit territories, and for iEMG decomposition. Moreover, we extend this model to a full multichannel iEMG simulator using classical linear EMG modelling and existing approaches to the generation of motor neuron discharge sequences. **Conclusions:** the obtained simulation model provides physiologically accurate MUAPs across entire motor unit territories and for various electrode configurations. **Significance:** it can be used for the development and evaluation of mathematical methods for multichannel iEMG processing and analysis.

Index Terms—EMG modelling, multichannel EMG, motor unit modelling, farthest point sampling.

I. INTRODUCTION

ITRAMUSCULAR EMG (iEMG) modelling supports the interpretation of the iEMG signal generation in human muscles. It permits to vary the parameters of both the motor neuron (MN) pool and the muscle fibers in order to test and validate iEMG-based computational methods, such as decomposition and motor unit (MU) territory estimation.

Different applications require simulation models of different complexities. For example, iEMG decomposition algorithms have been often tested using signals simulated with *phenomenological* EMG models [1]. These approaches involve the convolution of experimental or simulated MN spike trains with experimental motor unit action potentials (MUAPs) and provide known spike trains and adjustable levels of additive noise. However, they lack the modelling of the neuromuscular

TABLE I
MAIN ACRONYMS AND NOTATIONS

iEMG	Intramuscular EMG
MN	Motor neuron
MF	Muscle fiber
MU	Motor unit
MNAP	Motor neuron action potential
SFAP	Single fiber action potential
MUAP	Motor unit action potential
NMJ	Neuromuscular junction
FPS	Farthest point sampling
L	Length of the muscle
A	Area of the muscle cross-section
N, F, B, P, D	Total numbers of MNs (MUs), MFs, axon branches, observation points and electrode trajectory nodes
$\cdot_n, \cdot_f, \cdot_b, \cdot_p$	Indices designating a specific MN (MU), MF, axon branch and observation point
F_n, B_n	Numbers of MFs and axon branches in n -th MU
s_n, a_n	Size and innervation area of n -th motor neuron
$\phi_{fp}(t)$	SFAP of f -th MF in observation point p
$\Phi_{np}(t)$	MUAP of n -th MN in observation point p
$y_p(t)$	EMG signal in observation point p
$\mathbf{Y}_{\mathbf{E}}(t)$	EMG signal in multichannel electrode \mathbf{E} ; this and other symbols in bold designate matrices and vectors, instead of scalars

jitter, morphological variability of MUAPs, noise generated by distant MUs, and electrode geometry.

Compared to the phenomenological approach, *biophysical modelling* of iEMG includes the calculation of each single fiber action potential (SFAP) as a function of the fibers' morphology and of the electrode's relative position. This approach provides an infinitely wide dictionary of MUAPs, permits to take into consideration the electrode position and the neuromuscular jitter. Moreover, biophysical EMG simulation can be complemented by a force generation model in order to establish a complete model of the muscle electrical and mechanical responses [2], [3]. In this paper, we present a new biophysical MUAP simulation model.

In this paper, we target the simulation of MUAPs recorded by modern multichannel intramuscular electrodes, such as those described in [4]. This objective requires the biophysical approach to simulation, including modelling of the motor unit (MU) territories, neuromuscular junctions (NMJ) locations, and muscle fiber (MF) parameters. We also extend our approach to the modelling of gradually shifting intramuscular electrodes for the simulation of scanning recordings and evaluation of iEMG decomposition techniques.

Manuscript created July 1, 2019.

Konstantin Akhmadeev and Yannick Aoustin are with Université de Nantes, France. Tianyi Yu and Eric Le Carpentier are with École Centrale Nantes, France. Dario Farina is with Imperial College London, England (correspondence e-mail: d.farina@imperial.ac.uk).

Previous simulation models of iEMG have not been specifically developed for multichannel recordings since these recordings have been so far not common. Particularly, existing models [5], [6], [7] use constant distributions for the locations of the MN innervation centers and of MFs, which results in their non-uniform scattering in the muscle cross-section. Additionally, approach presented in [5] assigns an exact number of MFs to a motor neuron, forcing innervation of fibers at large distances from the theoretical innervation zone. While these issues minimally influence the surface or single-channel localized intramuscular recordings, we observed that it drastically affects the multichannel and scanning ones.

We have also observed that existing distributions of axial locations of the NMJs [5], [6] result in a large scattering of single fiber action potentials (SFAP) propagation delays. This causes MUAP waveforms to be too complex in the multichannel simulations and to vary too quickly in the scanning recordings.

In order to address these issues we propose a new modelling approach that modifies several aspects of previous modelling works, while preserving some of their properties [5], [8], [9], [7].

In comparison with existing approaches, specific novelties of our method are: 1) a new way to generate MFs coordinates and MN innervation centers; 2) controllable and robust method for fiber-neuron assignment; 3) an improved model of the terminal arborization of motor neuron axons; 4) multichannel and scanning electrode modelling. Although the proposed model focuses on the simulation of MUAPs, it can be easily extended to a full iEMG generation. This requires an appropriate motor neuron pool model for the spike trains generation, such as that presented in [6].

The remainder of this article is organized as follows. MFs and innervation centers distributions in the muscle cross-section are presented in section II-A. Next, the fiber-neuron assignment procedure is described in section II-A3. Section II-B4 explains the modelling of terminal arborizations and of MN action potential (MNAP) propagation delays. Finally, the simulation of MUAPs recorded by multichannel and scanning electrodes is described in section II-C6. Examples that demonstrate the performance of the proposed sub-models will be presented both in the Methods (II) and Results (III) sections.

II. METHODS

A. Model of the MF distribution and innervation

1) *Distribution of innervation centers in the cross-section of the muscle:* We assume that innervation centers of the motor neurons are distributed uniformly in the muscle cross-section. This assumption was also made in previous works on EMG simulation [6], [7]. Their authors propose to draw the innervation centers from a constant distribution over muscle cross-section. The issue arising from this approach is that constant distribution does not guarantee the resulting innervation centers to be uniformly scattered in the muscle cross-section.

We propose to use the farthest point sampling (FPS) [10], [11] instead of drawing from the constant distribution. FPS is a family of algorithms that fill a 2D domain by iteratively adding

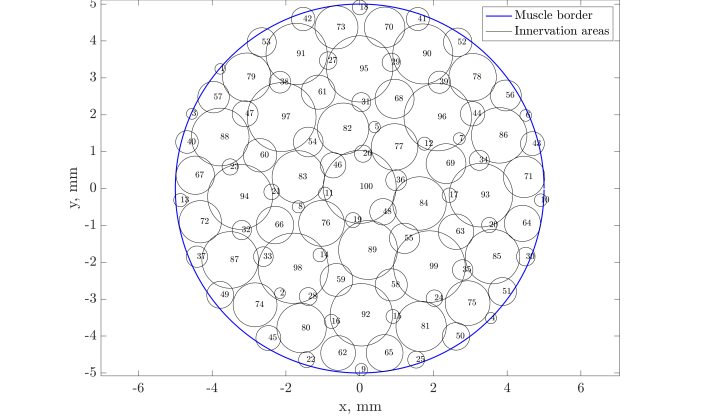


Fig. 1. Innervation centers of $N=100$ motor neurons (magnitude $R=50$) across the cross-section area of the muscle; circles are drawn to illustrate the sizes of corresponding MN (and not their innervation areas).

points that are maximally distant from the already added ones and from the region's borders. The FPS algorithms also permit to specify an arbitrary density function over the region [10], [11], [12].

The aforementioned property of FPS algorithms allows us to maximally disperse the motor neurons' innervation centers in the muscle cross-section. Moreover, by generating innervation centers in the order of decreasing motor neurons' sizes, we obtain a distribution in which the territories of motor neurons with similar sizes are as distant from each other as possible. As an example, Figure 1 shows that the innervation centers of different sizes evenly fill the muscle cross-section. We note that this property promotes the uniformity for distributions of the parameters that depend on MN size, e.g. muscle fiber diameters, a problem that was addressed in [13], [14]. Alternatively, motor neurons can be assigned in a randomized order, if the simulation strategy includes no specific assumptions on the innervation geometry.

2) *Distribution of fibers in the cross-section of the muscle:* Similarly to [5], [7], [15], MFs are modeled as straight parallel lines oriented along the z -axis, with their extremities located in the tendon regions, while the muscle is modeled as a cylinder.

The distribution of MFs in the muscle cross-section (xy -plane) should be uniform and, preferably, should take into consideration the diameters of fibers. In previous works [6], [7], the fibers' locations were drawn from a constant distribution within the corresponding motor unit territory. As it was noted above, this method, combined with previous approaches for innervation centers generation, does not guarantee the global uniformity in the entire muscle cross-section. Alternatively, in [5] MFs were positioned prior to the generation of innervation centers in the nodes of a regular rectangular grid.

We propose to generate the MFs locations using the FPS algorithm, prior to the generation of innervation centers, in order to obtain a distribution with guaranteed uniformity in the entire muscle cross-section. Figure 2 provides a comparison of the locations generated by this method with those drawn from the constant distribution. In our simulation we use constant MF density of 400 fibers per mm^2 , however, FPS additionally permits to impose a specific local density for each point of

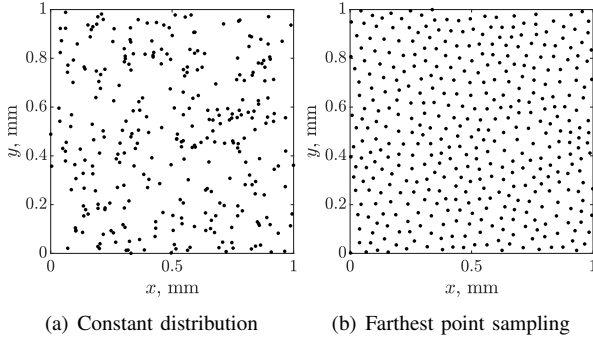


Fig. 2. MFs distribution in a 1-mm² area, generated by drawing from constant distribution (a) and by FPS (b).

the region.

3) *Fiber-neuron assignment*: We establish a randomized procedure in which fibers are assigned to motor neurons according to the following variables: the expected number of fibers innervated by the neuron, fiber's proximity to the innervation center and presence of neighboring fibers already assigned to that motor neuron. For each neuron-fiber pair, the probability of assignment is represented by a *score* that combines influences of each of these factors:

$$P_f(n) \sim P_n^a \cdot P_n^g(x_f, y_f) \cdot P_n^d(i, f, n_c) \quad (1)$$

where $P_f(n)$ is the score that characterizes the probability of f -th fiber to be assigned to n -th neuron; P_n^a denotes the *a priori* probability of assignment, P_n^g denotes the distribution of fiber's coordinates around n -th motor neuron, and $P_n^d(n, f, n_c)$ is an indicator function returning 0 if any of n_c closest neighbors of f -th fiber is already assigned to n -th unit, and 1 otherwise.

The pseudocode of the fiber assignment algorithm is presented in Algorithm 1. Let us consider each multiplier in (1) in a detailed way.

4) *A priori probability of assignment*: The number of MFs innervated by a motor neuron is proportional to its size. We calculate the *a priori* probability P_n^a of muscle fiber innervation in the following way:

$$P_n^a = \frac{s_n}{\sum_{n=1}^N s_n} \quad (2)$$

where s_n is the size of the n -th motor neuron which can be modeled using an exponential distribution for recruitment thresholds, as proposed in [6].

5) *Distribution of MF coordinates around an innervation center*: We assume that the innervation territories of MNs are circular; this assumption is common for EMG simulation models and is supported by experimental data [16]. We model the P_n^g as a symmetrical two-dimensional Gaussian distribution:

$$P_n^g(x, y) = \frac{1}{S_n} \cdot \frac{1}{2\pi\sigma_n^g} \exp \left[-\frac{(x - \mu_{nx}^g)^2 + (y - \mu_{ny}^g)^2}{2\sigma_n^{g2}} \right] \quad (3)$$

where x and y are coordinates of the muscle fiber; mean μ_i^g is coincident with the innervation center of n -th motor neuron; S_n is an out-of-border coefficient (see explanation below in

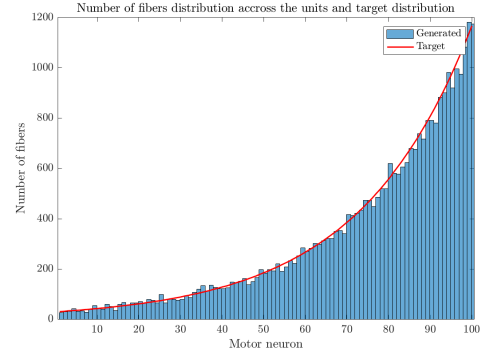


Fig. 3. Number of fibers innervated by each motor neuron for a muscle with radius of 5 mm, 31400 fibers, $N=100$ neurons and magnitude of size distribution $s_N/s_1=50$. Red curve: model, according to motor neuron sizes; bar plot: proposed assignment procedure.

this section); standard deviation $\sigma_n^g = a_n/\pi C$ is proportional to the MN's innervation area a_n with scattering coefficient C .

We assume that innervation areas of MNs are proportional to their sizes, with a scaling factor A/k : $a_n = s_n/s_N \cdot A/k$, where A is the area of the muscle cross-section. The value of k sets up the area of the largest MN as a fraction of the muscle cross-section area: $k = A/a_N$. The value of k varies across muscles. In our simulation, we have chosen a value of $k=4$. The value of the scattering coefficient C regulates the tightness of the Gaussian distribution of fibers around the innervation center. We calculate it assuming that a_n is the area of 0.99 confidence circle for corresponding distribution, giving us $C = \text{inv-}\chi^2(0.99, 2) = 9.21$.

Out-of-border coefficient S_n takes into consideration the fact that innervation areas of some motor neurons may exceed the muscle border, which, in reality, should not make them innervate less MFs than required by their size. S_n is calculated as a double integral of the original Gaussian distribution in (3) above the domain corresponding to the muscle cross-section. Thus, the probability P_n^g sums to 1 while integrating over the muscle region. Considering the classification proposed in [13], this approach can be assigned to *uniform-augmented* territory placement.

6) *Adjacency of fibers innervated by same motor neuron*: Due to the phenomenon of self-avoidance in the arborizations of MNs axons [17], MFs of the same motor unit rarely lie next to each other. This fact is reflected in equation (1) by using an additional factor $P_n^d(n, f, n_c)$, which equals to zero if at least one of the n_c closest fibers is already innervated by n -th motor neuron.

The value of n_c also regulates the scattering of MNs' fibers across the muscle cross-section. We suggest $n_c = 5$ for a regular modelling strategy. This choice prevents the formation of dense clusters of fibers innervated by the same MN, while authorizing a limited adjacency.

7) *Results of the MFs innervation modelling*: In order to demonstrate the results of the fiber innervation model, we simulated a muscle of 10 mm in diameter with a mean fiber density of 400/mm², resulting in approximately $F=34000$ fibers. It was innervated by $N=100$ motor neurons with mag-

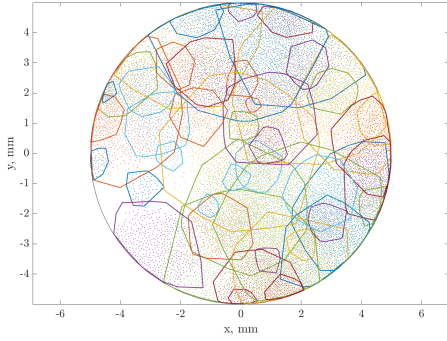


Fig. 4. Innervation territories of MNs from the same simulation as in Figure 3, drawn as convex hulls of innervated fibers coordinates; a random subset of 50 out of 100 MN is shown to avoid clutter. Points of the same color as borders represent the innervated MFs' locations.

Algorithm 1 Fiber assignment procedure

```

1: while not all fibers are assigned do
2:    $w = \text{zeros}(N,1)$ ;
3:    $f = \text{random non-assigned fiber}$ ;
4:   for each motor neuron  $n$  do
5:     calculate  $P_n^a, P_n^g, P_n^d$ ;
6:      $w_n \leftarrow P_n^a \cdot P_n^g \cdot P_n^d$ ;
7:   end for
8:   assign fiber  $f$  to a random neuron  $n$  with weight  $w_n$ ;
9: end while

```

nitude of size distribution $s_N/s_1=50$. The resulting numbers F_n of innervated fibers per motor neuron are shown in Figure 3. This distribution follows very closely the one imposed by the model $F_n = F \cdot s_n / \sum_{n=1}^N s_n$.

The resulting innervation areas also lie close to their model-imposed values. They can be calculated both as areas of convex hulls or areas of 0.99 confidence ellipsoids. An example of resulting innervation territories' forms is provided in Figure 4.

B. Model of the axon branching

A neuromuscular junction is a biological interface between a single muscle fiber and its innervating motor neuron axon. In order to innervate all its fibers, an axon splits into smaller branches, forming a complex and uneven tree structure with neuromuscular junctions at its leaves [17].

The motor neuron action potential (MNAPs) originates in the soma of the MN and propagates along the MN axon branches until reaching each of the innervated MFs. The lengths of the paths to each fiber vary due to the scattering of the neuromuscular junctions in the muscle. This causes the scattering of MNAP propagation delays, which affects the morphology of the MUAPs. As concluded in [16], temporal dispersion of the MUAPs is to a larger extent due to the spatial dispersion of the NMJs than to the differences in conduction velocities of the fibers.

In this section, we will show how our simulation model calculates the coordinates of neuromuscular junctions and MNAP propagation delays.

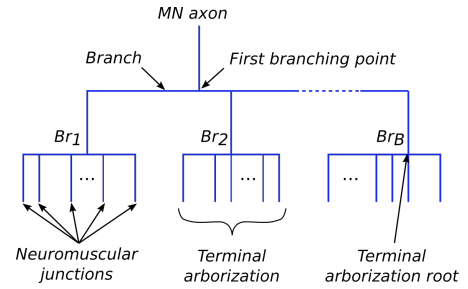


Fig. 5. Structure of motor neuron axon branching, modeled as a tree with a single bifurcation, where the axon is the root and neuromuscular junctions are the leaves. Leaves are organized into terminal arborizations Br_i using k -means clustering of fiber positions in the cross-sectional plane.

1) *Structure of the axon branching model:* A MN axon can be represented as a root of a tree structure that splits into several branches of smaller radii. This process is then repeated several times within each branch until each muscle fiber is reached.

In our model, we suppose that split is done only twice (see Figure 5). Thus, each muscle fiber and its neuromuscular junction are assigned not only to a motor neuron but to a specific branch of its axon. We establish such a model in order to constrain the complexity of MUAPs while providing physiologically correct distributions of NMJs along the muscles.

2) *Fiber-branch assignment:* We assume that the number of branches is proportional to the MU's size and that its value defines the number of phases in its action potential. The following expression provides the numbers of branches/phases that correspond to the experimental action potentials for small motor units (1-2 phases) as well as for the largest ones (4-6 phases):

$$B_n = 1 + \lfloor \ln(s_n/s_1) \rfloor \quad (4)$$

where s_n is size of n -th motor unit and $\lfloor \cdot \rfloor$ stands for rounding to the nearest integer.

For each motor unit, in order to assign each MF to a specific branch, we first define the number B_n of branches using equation (4) and then run the k -means clustering algorithm over the motor unit's fibers coordinates in the cross-sectional plane, looking for B_n clusters. In this case, k -means seeks for B_n groups of closely-located MFs of the MU. Then the MFs of each group are assigned to a single axon branch.

3) *Coordinates of neuromuscular junctions:* In the muscle cross-section (xy -plane), the NMJs coincide with their MFs. Along the z -axis, the assignment of the MFs to specific axon branches permits to generate a multi-modal distribution of the NMJs (see Figure 6). Such distribution has an advantage over previously used uniform or unimodal Gaussian distributions [5] in terms of MUAP waveforms, especially in case of large MUs, where unimodal distributions tend to excessively scatter the SFAP delays, leading to the generation of abnormally polyphasic MUAPs.

Figure 6 demonstrates the distribution of MFs of two different branches in the cross-sectional area (left), as well as the densities of their neuromuscular junctions along the z -axis (right). These densities are modeled as Gaussian clusters

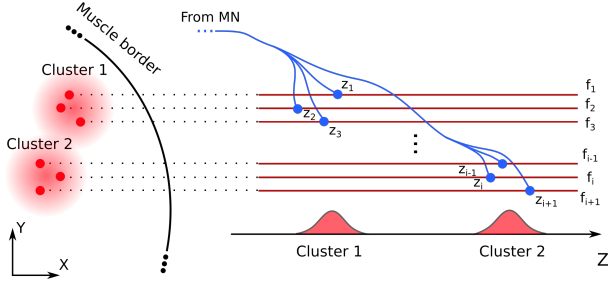


Fig. 6. Neuromuscular junction z-coordinates distribution model: combination of Gaussians scattered across end-plate zone, each associated with a cluster of MFs in the muscle cross-section.

with mean values scattered across the z -axis of the muscle, and standard deviations much smaller than the muscle length.

We calculate mean values μ_n^b and standard deviations σ_n^b of intra-cluster densities using the following model:

$$\begin{aligned} \mu_n^b &\sim g(L/2, \sigma_n), \quad \sigma_n = a_\mu + b_\mu \cdot \sum_{k=1}^n s_k / \sum_{k=1}^N s_k \\ \sigma_n^b &= a_\sigma + b_\sigma \cdot \sum_{k=1}^n s_k / \sum_{k=1}^N s_k \end{aligned} \quad (5)$$

where parameters a_μ , b_μ , a_σ , b_σ in combination with fiber and axon conduction velocities define the dispersion of the MNAP propagation delays, and, thus, the duration of MUAPs.

In order to obtain an initial estimate of these parameters, we impose the largest and the smallest MUs to have MUAPs with durations of 2.5 ms and 7.5 ms respectively. Considering mean conduction velocities of their fibers to be 2500 mm/s and 5000 mm/s [9], we can approximately calculate the necessary span of their neuromuscular junctions, giving correspondingly $l_{min} = 6.25$ mm and $l_{max} = 37.5$ mm. We also assume that the standard deviation of the cluster centers σ_n is larger than the intra-cluster deviation σ_n^b since a MUAP usually contains several distinct phases. In simulation, we have found that it is convenient to set $d_\sigma = \sigma_n / \sigma_n^b$ to 4. Finally, we note that the span of neuromuscular junctions along the z -axis for n -th motor unit can be roughly calculated as $3(\sigma_n + \sigma_n^b)$.

These considerations give us the following system of equations:

$$\begin{cases} 3(a_\mu + a_\sigma) = l_{min}, \\ 3(a_\mu + a_\sigma + b_\mu + b_\sigma) = l_{max}, \\ b_\mu / b_\sigma = d_\sigma, \\ a_\mu / a_\sigma = d_\sigma; \end{cases} \quad (6)$$

solution of which for $d_\sigma = 4$ gives $a_\sigma = 0.4$, $b_\sigma = 2.1$, $a_\mu = 1.7$, $b_\mu = 8.3$ (all in millimeters). We should consider these values as upper estimates, since MUAPs' lengths are also influenced by MNAP propagation delays (see Section II-B4 for details) which were not yet taken into account. According to our observations and for MNAP propagation delays listed in Section II-B4, a set $a_\sigma = 0.25$, $b_\sigma = 1$, $a_\mu = 1$, $b_\mu = 2.5$ produces MUAPs with physiologically correct forms and duration.

4) *Delay of MNAP propagation*: Once all the MFs of a motor unit are assigned to their branches and the z -coordinates of NMJs are generated, we can calculate the delays of MNAP propagation towards each junction. We divide the lengths of each segment of the axon (see Figure 5) by their propagation velocities, thus, the delay for f -th fiber assigned to b -th branch of n -th motor unit is:

$$d_f = \frac{|\mathbf{x}_n^c - \mathbf{x}_k^b|}{v_b} + \frac{|\mathbf{x}_k^b - \mathbf{x}_f^j|}{v_t} \quad (7)$$

where

- \mathbf{x}_f^j are coordinates of the neuromuscular junction of f -th fiber in k -th branch of n -th motor unit.
- \mathbf{x}_k^b are coordinates of the terminal arborization root at the k -th branch of the n -th motor neuron's axon, calculated as mean of the neuromuscular junctions positions:

$$\mathbf{x}_k^b = \sum_{f=1}^{N_k} \mathbf{x}_f^j$$

- \mathbf{x}_n^c are coordinates of the first branching point of n -th motor unit, which is calculated as the mean of arborization roots:

$$\mathbf{x}_n^c = \sum_{k=1}^{K_n} \mathbf{x}_k^b$$

- v_b is MNAP propagation velocity in a branch of the motor neuron axon;
- v_t is MNAP propagation velocity in a terminal arborization of the motor neuron axon;

We assume that branches' propagation velocities are much smaller than that of the axon due to their smaller diameter and the absence of myelination in case of terminal arborization. Values that we used in our model are: $v_b = 10$ m/s, $v_t = 1$ m/s (for comparison, typical propagation velocity of an MN axon is 50 m/s). To our best knowledge, there is yet no experimental data on v_t and v_b in the literature.

C. MUAP and EMG simulation

1) *Muscle fiber action potential modelling*: In order to simulate single fiber action potentials (SFAPs) we define a potential induced in an observation point by an elementary current source located at a narrow fiber's slice at coordinate z [18], [9]:

$$\phi_p = \frac{d}{4\sigma_r} \cdot \frac{I_e}{\sqrt{r^2\sigma_r/\sigma_z + (z_p - z)^2}} = h(z_p - z)I_e \quad (8)$$

where

- I_e is an elementary current source;
- z and z_p are locations of the elementary current source and of the observation point respectively;
- r is radial distance between the muscle fiber and the observation point;
- d is the diameter of the muscle fiber; values of the diameters are modeled as proposed in [5];
- σ_r and σ_z are radial and axial conductivities of the muscle tissue (0.063 S/m and 0.33 S/m respectively [9]);

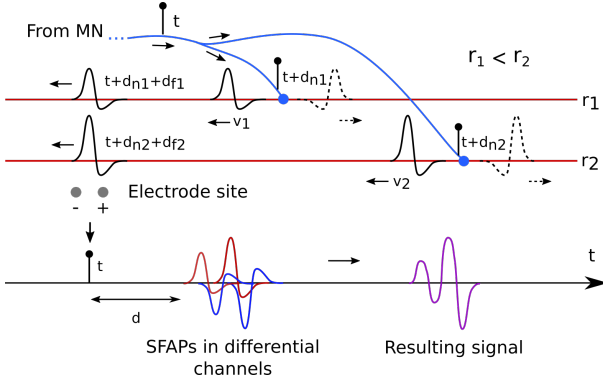


Fig. 7. Effect of propagation delays of MNAPs (d_n) and SFAPs (d_f) on resulting motor unit action potential.

During contraction, transmembrane current sources are continuously distributed along the fiber rather than being concentrated in certain points. Let us denote this distribution, at time t , as $I(z, t)$. The potential $\phi_p(t)$ at the observation point p , generated by this distribution can be calculated as convolution [9]:

$$\phi_p(t) = \int_{-\infty}^{\infty} h(z_p - z)I(z, t) dz \quad (9)$$

In order to model the transmembrane current distribution $I(z, t)$, we use the approach proposed in [8] (see their equation (17)), which was also recently implemented in another EMG simulation model [7]. The intracellular action potential model from [9] was used, as suggested in [19].

2) *Motor unit action potential modelling*: Action potential of a MU is modeled as a linear sum of its muscle fibers' SFAPs [5]. Taking in consideration the delays and neuromuscular jitter in axon branches (see also Figure 7 for illustration):

$$\Phi_{np}(t) = \sum_{f=1}^{F_n} \phi_{fp}(t - d_f - \zeta) \quad (10)$$

where $\Phi_{np}(t)$ is the MUAP of n -th motor unit, observed in point p ; F_n is number of fibers innervated by this motor unit; $\phi_{fp}(t)$ is SFAP of f -th muscle fiber of n -th motor unit, observed in point p ; d_f is the delay between the MNAP discharge and its arrival to the neuromuscular junction of the fiber (see expression (7)); ζ is a neuromuscular delay caused by jitter, randomly drawn for each muscle fiber and for each new realization of Φ_{ip} .

Delays caused by neuromuscular jitter are of the order of μs [20]. In order to be able to simulate their influence on the SFAPs, while using reasonable sampling frequencies, we use sub-sample waveform shifting presented in [21].

3) *EMG in a single observation point*: EMG is modeled as a linear sum of contributions from all MUs [22], while the contributions are convolutions of spike trains and MUAPs. We formulate the expression for simulated EMG, acquired in observation point p , in a similar way:

$$y_p(t) = \sum_{n=1}^N \sum_{k=1}^{\text{card}(U_n)} \Phi_{np}(t - U_{nk}) \quad (11)$$

where $y_p(t)$ is the simulated EMG signal in observation point p , U_n is a vector of spikes' time instants for n -th motor neuron; and k is the index of a spike in U_n .

4) *EMG in a single-channel electrode*: Due to the fact that a metallic electrode is a conductor, the electric potential is constant across its volume. Its value can be approximated by an average field in the observation points adjacent to the electrode [5]. Therefore, a SFAP detected by an electrode can be calculated as an integral of the potential $\phi(t)$ over the electrode's surface. Due to the linearity of (10) and (11), the same applies to MUAPs and the overall signal detected by the electrode.

In our model, we approximate the recording surface by a number of elements with an observation point associated to the center of each element. The electrode potential is, thus, equal to the sum of element potentials weighted by their areas. Thus, iEMG signal recorded by an electrode is a linear combination of the signals in the observations points:

$$\mathbf{Y}_{\mathbf{E}}(t) = [\pm e_1 \quad \pm e_2 \quad \dots \quad \pm e_P] \cdot \begin{bmatrix} y_1(t) \\ y_2(t) \\ \dots \\ y_P(t) \end{bmatrix} = \mathbf{E}\mathbf{Y}(t) \quad (12)$$

where e_p is area of the electrode's element associated to p -th observation point, its sign depends on the polarity of corresponding amplifier input; $y_p(t)$ is EMG signal calculated at observation point p using equation (11); in following, \mathbf{E} and $\mathbf{Y}(t)$ will be referred to as *electrode matrix* and *observation vector*. See examples in the appendix.

MUAP recorded by electrode \mathbf{E} can be easily obtained using (11) and (12) while setting $U_n = \{0\}$:

$$\Phi_{n\mathbf{E}} = [\pm e_1 \quad \pm e_2 \quad \dots \quad \pm e_P] \cdot \begin{bmatrix} \Phi_{n1}(t) \\ \Phi_{n2}(t) \\ \dots \\ \Phi_{nP}(t) \end{bmatrix} = \mathbf{E}\Phi_n(t) \quad (13)$$

This holds as well of the following equations of multichannel and scanning recordings.

5) *EMG in a multichannel electrode*: Calculation of a multichannel EMG signal can be conveniently represented by a stack of electrode matrices \mathbf{E} (12):

$$\mathbf{Y}_{\mathbf{E}}(t) = \begin{bmatrix} \mathbf{E}_1 \\ \mathbf{E}_2 \\ \dots \\ \mathbf{E}_M \end{bmatrix} \begin{bmatrix} y_1(t) \\ y_2(t) \\ \dots \\ y_P(t) \end{bmatrix} = \mathbf{E}\mathbf{Y}(t) \quad (14)$$

6) *Modelling of EMG in a shifting electrode*: Shifts can be modeled as a combination of translations and rotations of the electrode along a specified trajectory in the muscle. This trajectory can be approximated by a number of *nodes* D linked by successive rigid transformations.

The current position of the electrode on the trajectory curve can be specified by a continuous path parameter $0 \leq \lambda \leq D - 1$, where D denotes the overall number of nodes in the trajectory.

The signal, as a function of the current position of the electrode, can be calculated as follows:

$$\mathbf{Y}_{\mathbf{E}}(t, \lambda) = \mathbf{E} [\mathbf{I}_1(\lambda) \mathbf{I}_2(\lambda) \dots \mathbf{I}_D(\lambda)] \begin{bmatrix} \mathbf{Y}^1(t) \\ \mathbf{Y}^2(t) \\ \dots \\ \mathbf{Y}^D(t) \end{bmatrix} \quad (15)$$

where $\mathbf{I}_d = \mathbf{I} \cdot \delta(\lambda - (d - 1))$, $\delta(\cdot)$ is Dirac delta function and \mathbf{I} is identity matrix of size P ; $\mathbf{Y}^d(t)$ is the observation vector in the trajectory node d .

The signal acquired in positions located between the trajectory nodes can be linearly interpolated, given a sufficiently fine trajectory sampling. One can express the signal acquired in a specific position λ on the trajectory:

$$\mathbf{Y}_{\mathbf{E}}(t, \lambda) = \mathbf{E} [\hat{\mathbf{I}}_1(\lambda) \hat{\mathbf{I}}_2(\lambda) \dots \hat{\mathbf{I}}_D(\lambda)] \begin{bmatrix} \mathbf{Y}^1(t) \\ \mathbf{Y}^2(t) \\ \dots \\ \mathbf{Y}^D(t) \end{bmatrix} \quad (16)$$

where $\hat{\mathbf{I}}_d(\lambda)$ is a weighted identity matrix determined as following:

$$\hat{\mathbf{I}}_d(\lambda) = \mathbf{I} \cdot \max[0, 1 - |d - 1 - \lambda|] \quad (17)$$

Kernel (17) is equal to one when $\lambda = d - 1$ (i.e. when calculating the signal exactly in trajectory node d) and linearly weights the neighbouring nodes d and $d + 1$ when $d - 1 < \lambda < d$. An example of a MUAP captured by a fine-wire electrode, that moved transversally to the MFs, is shown in Figure 8.

Path parameter λ can be a function of force or time since usually electrode shifts occur due to either muscle deformation during contraction or other factors that can be described as functions of time.

III. SIMULATION RESULTS

In order to demonstrate the capabilities of the proposed model, we provide several examples of how it can be applied to the simulation of experimental studies.

A. Multichannel MUAP example

To assess the performance of the proposed multichannel MUAP modelling, we establish a simulation case showed in Figure 8: an array of 16 equidistant electrodes spaced by 1 mm gap was inserted into the muscle at the angle of 30 degrees to the fibers. This array simulates recently proposed intramuscular electrodes for human studies [4]. In total, 15 channels were obtained by consecutive differentiation of the signals in the electrodes. We have chosen a MU for which the center of the territory lied close to the electrodes. The length of the muscle in this simulation was 50 mm, and the end-plate zone was positioned around the center of the muscle, as stated in formula (5). The array was placed in one of the halves of the muscle and didn't cross the MU's end-plate zone.

From Figure 8, we notice several relevant results. First, the amplitudes of the MUAPs are inversely proportional to the distance between the channel's observations points and the center of the MU's territory. Second, the centers of energy of the MUAPs shift to the right as the distance between the channel and the end-plate increases, due to the simulation of SFAP conduction. Third, the transformations between MUAPs in neighboring channels are consistent and MUAPs have physiologically correct durations (approximately 5 ms).

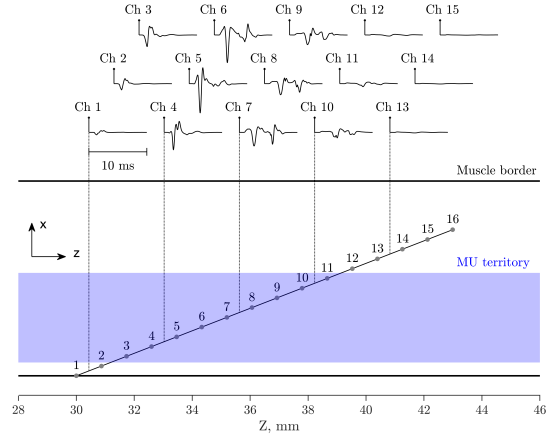


Fig. 8. Lower half: multichannel array of 16 equidistant electrodes spaced by 1 mm gap, inserted into the muscle at the angle of 30 degrees to the fibers. Consecutive differentiation is applied to the multichannel signal, providing 15 differential channels. Upper half: MUAPs in each of the resulting 15 differential channels. All MUAP plots have the same vertical axis scale. The black round markers designate the trigger time, same for all the MUAP plots.

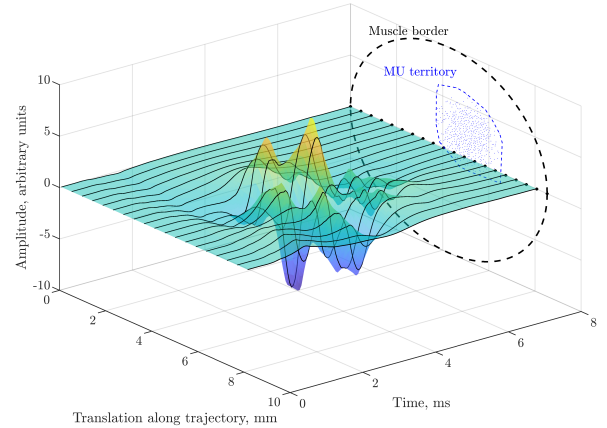


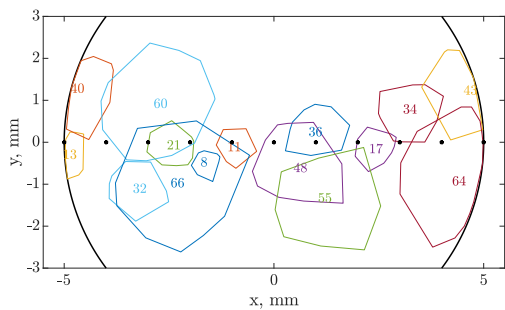
Fig. 9. A scan simulated with a two-point differential electrode which was shifted transversally along a 10 mm-long trajectory across the territory of a MU. Black dots on the right plane are 1 mm increments of the electrode position, for which the MUAPs (black solid lines) are calculated. Intermediate values of MUAPs are obtained using scanning and interpolation formula (16).

B. Single MU territory scanning simulation

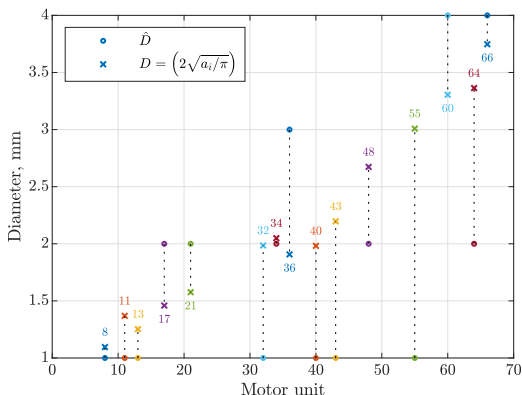
Equation (16) permits to simulate a "scan" of a motor unit territory. An example is presented in Figure 9 where a MUAP is shown at 10 equidistant nodes positioned along a straight trajectory that goes across a large MU's territory through its center. The overall duration of the generated MUAP is approximately 5 ms. This result is qualitatively in agreement with experimental observations [23], [24].

C. MUs territory assessment

The multichannel MUAP model permits to simulate the studies that aim at the estimation of MUs' innervation territories. As an example, here we have simulated a procedure that is similar to a previous experimental study [25]. More specifically, we have simulated a 10-mm long array of 11



(a) Location of the innervation territories of detectable MUs in the cross-section of the muscle. Black dots - electrode locations, numbers - indices of MUs, colored lines - territories' borders.



(b) Estimated (\hat{D} , circles) and true (D , crosses) diameters of MU territories.

Fig. 10. Results of territory assessment simulation. Colors between figures are matched for easier correspondence.

equally spaced intramuscular electrodes, making ten channels with consecutive differentiation, inserted to a 10-mm wide muscle at an angle of 90° to the fibers. The diameters of the territories are estimated as the number of the channels where the MUAP's peak was four times greater than the standard deviation of the baseline noise [26], [25]. The SNR was set to 15 dB in this study. Only MUs with recruitment thresholds that are below of 50% MVC were considered for the analysis. In order to establish this limit, contraction force was calculated using the model proposed in [6].

From Figure 10, the estimated diameters generally correlate with their true values. However, this simulation highlights the fact that, for most of the MUs, the electrode array does not cross the center of their innervation territories, which results in an underestimation of the diameters (e.g., see MUs 40, 43, 55 in Figure 10). Also, we note that this technique limits the estimated diameters to be multiples of the inter-electrode distance and, thus, has low resolution. The proposed simulation model can be used to test and evaluate more complex approaches to MU territory assessment based on multichannel iEMG decomposition.

D. Multichannel iEMG decomposition

Finally, we present the results of the application of a decomposition algorithm to the simulated signals. In order

to generate an iEMG signal for decomposition, we have implemented the motor neuron pool model proposed in [6].

A linear array of five electrodes (1-mm interelectrode distance) with consequent differentiation, providing four iEMG channels, was used for this simulation. We measured the average power of the simulated signal in all channels at maximal net excitation in order to obtain a reference value for calculation of the standard deviation σ of the additive noise. MUAPs whose maximal absolute value exceeded 4σ in at least one of the four channels were considered detectable and their MUs were included to the annotation of the signal. The SNR in all channels was set to 15dB and a trapezoidal contraction reaching 20% MVC was generated.

The simulated EMG signal was decomposed by MTL, the multichannel version of the algorithm proposed in [27], [28]. We have compared the simulated annotation with the decomposition provided by MTL. The decomposition was evaluated using classification phase sensitivity and positive predictivity [29] averaged across 11 detected MUs, which resulted in, respectively, 0.93 ± 0.04 and 0.97 ± 0.03 .

This result shows that MUAPs simulated by the proposed model are conform to the feature extraction phase of a common existing decomposition algorithm. They also fit its multichannel model, providing results that are consistent in terms of the sensitivity and positive predictivity rates.

IV. DISCUSSION AND CONCLUSION

We have described a new model for MUAP simulation that includes the possibility to simulate multichannel intramuscular electrodes, their arbitrary positioning, and gradual shifting during acquisition. The model also includes new methods for establishing uniform distributions of muscle fibers and innervation centers in the muscle cross-section, for tuning the fiber-neuron assignment, and for controlling the complexity of the MUAPs.

While the model has several parameters to tune, these parameters are designed to reflect the physiology of the motor system and thus can be selected according to known physiological variables. We suggest that the proposed approach, being simple and physiology-based, provides greater flexibility of simulation configurations than previous models, especially in cases when different electrode types and placements are of interest.

This model can be used to simulate a wide range of experimental studies and computational methods, such as for MU territory estimation, conduction velocity assessment, denervation, and reinnervation. A full iEMG simulation has also been obtained by convolution of the modelled MUAPs with spike trains provided by a previous model of the motor neuron pool behaviour. This extension can be used for the assessment of decomposition algorithms in terms of their robustness towards the MUAPs variations.

In conclusion, we proposed a new model for the simulation of invasive multi-channel EMG recordings that have a wide range of potential applications in the test of computational methods applied to intramuscular EMG signals. The corresponding code can be accessed in the authors' online repository [30].

APPENDIX A
EXAMPLES OF THE ELECTRODE MATRIX FOR BASIC
SIMULATION CASES

A fine wire electrode can be approximated by a pair of points with equal areas. In the case of bipolar acquisition, the resulting signal is equal to the difference between potentials observed in the two points (see expression (12)):

$$\mathbf{Y}_{\mathbf{E}}(t) = \begin{bmatrix} 1 & -1 \end{bmatrix} \cdot \begin{bmatrix} y_1(t) \\ y_2(t) \end{bmatrix}$$

Signal acquired by an array of point electrodes with consecutive differentiation can be represented as follows (see expression (14)):

$$\mathbf{Y}_{\mathbf{E}}(t) = \begin{bmatrix} -1 & 1 & 0 & \dots & 0 \\ 0 & -1 & 1 & \dots & 0 \\ & & \dots & & \\ 0 & \dots & & -1 & 1 \end{bmatrix} \begin{bmatrix} y_1(t) \\ y_2(t) \\ \dots \\ y_P(t) \end{bmatrix}$$

Assuming that the electrode's trajectory is approximated by only two nodes, an EMG signal from a fine-wire electrode, before the shift ($\lambda = 0$) and after the shift ($\lambda = 1$) can be expressed as (see equation (15)):

$$\mathbf{Y}_{\mathbf{E}}(t, 0) = \begin{bmatrix} 1 \\ -1 \\ 0 \\ 0 \end{bmatrix}^{\top} \begin{bmatrix} y_1^1(t) \\ y_1^1(t) \\ y_2^2(t) \\ y_2^2(t) \end{bmatrix}, \mathbf{Y}_{\mathbf{E}}(t, 1) = \begin{bmatrix} 0 \\ 0 \\ 1 \\ -1 \end{bmatrix}^{\top} \begin{bmatrix} y_1^1(t) \\ y_1^1(t) \\ y_2^2(t) \\ y_2^2(t) \end{bmatrix}$$

where the lower index of y corresponds, as previously, to the electrode element, while its upper index denotes the trajectory node.

Applying expression (16) to the previous example, we can calculate the signal acquired at 1/4-th of the way ($\lambda = 0.25$):

$$\mathbf{Y}_{\mathbf{E}}(t, 0.25) = \begin{bmatrix} 0.75 \\ -0.75 \\ 0.25 \\ -0.25 \end{bmatrix}^{\top} \begin{bmatrix} y_1^1(t) \\ y_2^1(t) \\ y_1^2(t) \\ y_2^2(t) \end{bmatrix}$$

REFERENCES

- [1] D. Farina, A. Crosetti, and R. Merletti, "A model for the generation of synthetic intramuscular EMG signals to test decomposition algorithms," *IEEE Trans. on Biomedical Engineering*, vol. 48, no. 1, pp. 66–77, 2001.
- [2] J. L. Dideriksen, D. Farina, and R. M. Enoka, "Influence of fatigue on the simulated relation between the amplitude of the surface electromyogram and muscle force," *Philosophical Trans. of the Royal Society A: Mathematical, Physical and Engineering Sciences*, vol. 368, no. 1920, pp. 2765–2781, Jun. 2010.
- [3] G. Venugopal, P. Deepak, D. M. Ghosh, and S. Ramakrishnan, "Generation of synthetic surface electromyography signals under fatigue conditions for varying force inputs using feedback control algorithm," *Proc. of the Institution of Mechanical Engineers, Part H: J. of Engineering in Medicine*, vol. 231, no. 11, pp. 1025–1033, Nov. 2017.
- [4] S. Muceli, W. Poppendieck, F. Negro, K. Yoshida, K. P. Hoffmann, J. E. Butler, S. C. Gandevia, and D. Farina, "Accurate and representative decoding of the neural drive to muscles in humans with multi-channel intramuscular thin-film electrodes: Multi-channel intramuscular EMG electrode," *J. of Physiology*, vol. 593, no. 17, pp. 3789–3804, 2015.
- [5] A. Hamilton-Wright and D. Stashuk, "Physiologically Based Simulation of Clinical EMG Signals," *IEEE Trans. on Biomedical Engineering*, vol. 52, no. 2, pp. 171–183, Feb. 2005.
- [6] A. J. Fuglevand, D. A. Winter, and A. E. Patla, "Models of recruitment and rate coding organization in motor-unit pools," *J. of neurophysiology*, vol. 70, no. 6, pp. 2470–2488, 1993.
- [7] E. Petersen and P. Rostalski, "A comprehensive mathematical model of motor unit pool organization, surface electromyography, and force generation," *Frontiers in Physiology*, vol. 10, p. 176, 2019.
- [8] D. Farina, "A Novel Approach for Precise Simulation of the EMG Signal Detected by Surface Electrodes," *IEEE TRANSACTIONS ON BIOMEDICAL ENGINEERING*, vol. 48, no. 6, p. 10, 2001.
- [9] S. D. Nandedkar and E. Stalberg, "Simulation of single muscle fibre action potentials," *Medical & Biological Engineering & Computing*, vol. 21, no. 2, pp. 158–165, Mar. 1983.
- [10] G. Peyré, "Numerical Mesh Processing," Apr. 2008, course notes.
- [11] Y. Eldar, M. Lindenbaum, and M. Porat, "The Farthest Point Strategy for Progressive Image Sampling," *IEEE Trans. on Image Processing*, vol. 6, no. 9, p. 11, 1997.
- [12] G. Liang, L. Lu, Z. Chen, and C. Yang, "Poisson disk sampling through disk packing," *Computational Visual Media*, vol. 1, no. 1, pp. 17–26, Mar. 2015.
- [13] J. Navallas, A. Malanda, L. Gila, J. Rodriguez, and I. Rodriguez, "Comparative evaluation of motor unit architecture models," *Medical & Biological Engineering & Computing*, vol. 47, no. 11, pp. 1131–1142, Nov. 2009.
- [14] J. Navallas, A. Malanda, L. Gila, J. Rodriguez, and I. Rodriguez, "A muscle architecture model offering control over motor unit fiber density distributions," *Medical & Biological Engineering & Computing*, vol. 48, no. 9, pp. 875–886, Sep. 2010.
- [15] D. Farina and A. Rainoldi, "Compensation of the effect of sub-cutaneous tissue layers on surface EMG: A simulation study," *Medical Engineering & Physics*, vol. 21, no. 6-7, pp. 487–497, Jul. 1999.
- [16] F. Buchthal, C. Guld, and P. Rosenfalck, "Multielectrode Study of the Territory of a Motor Unit," *Acta Physiologica Scandinavica*, vol. 39, no. 1, pp. 83–104, Jan. 1957.
- [17] D. A. Gibson and L. Ma, "Developmental regulation of axon branching in the vertebrate nervous system," *Development*, vol. 138, no. 2, pp. 183–195, Jan. 2011.
- [18] R. Plonsey, "The Active Fiber in a Volume Conductor," *IEEE Trans. on Biomedical Engineering*, p. 11, 1974.
- [19] J. Duchene and J.-Y. Hogrel, "A model of EMG generation," *IEEE Trans. on Biomedical Engineering*, vol. 47, no. 2, pp. 192–201, Feb. 2000.
- [20] J. Ekstedt, G. Nilsson, and E. Stlberg, "Calculation of the electromyographic jitter," *J. of Neurology, Neurosurgery & Psychiatry*, vol. 37, no. 5, pp. 526–539, 1974.
- [21] K. C. McGill and L. J. Dorfman, "High-Resolution Alignment of Sampled Waveforms," *IEEE Trans. on Biomedical Engineering*, vol. BME-31, no. 6, pp. 462–468, Jun. 1984.
- [22] D. Farina, A. Crosetti, and R. Merletti, "A model for the generation of synthetic intramuscular EMG signals to test decomposition algorithms," *IEEE Trans. on Biomedical Engineering*, vol. 48, no. 1, pp. 66–77, 2001.
- [23] E. Stalberg and L. Antoni, "Electrophysiological cross section of the motor unit," *J. of Neurology, Neurosurgery & Psychiatry*, vol. 43, no. 6, pp. 469–474, Jun. 1980.
- [24] J. Navallas and E. Stalberg, "Studying motor end-plate topography by means of scanning-electromyography," *Clinical Neurophysiology*, vol. 120, no. 7, pp. 1335–1341, Jul. 2009.
- [25] B. L. Luu, S. Muceli, J. P. Saboisky, D. Farina, M. E. Hroux, L. E. Bilston, S. C. Gandevia, and J. E. Butler, "Motor unit territories in human genioglossus estimated with multichannel intramuscular electrodes," *J. of Applied Physiology*, vol. 124, no. 3, pp. 664–671, 2018.
- [26] M. E. Hroux, H. J. Brown, J. T. Inglis, G. P. Siegmund, and J.-S. Blouin, "Motor units in the human medial gastrocnemius muscle are not spatially localized or functionally grouped," *J. of Physiology*, vol. 593, no. 16, pp. 3711–3726, 2015.
- [27] J. Florestal, P. Mathieu, and A. Malanda, "Automated decomposition of intramuscular electromyographic signals," *IEEE Trans. on Biomedical Engineering*, vol. 53, no. 5, pp. 832–839, May 2006.
- [28] K. C. McGill, Z. C. Lateva, and H. R. Marateb, "EMGLAB: an interactive EMG decomposition program," *J. of Neuroscience Methods*, vol. 149, no. 2, pp. 121–133, Dec. 2005.
- [29] D. Farina, R. Colombo, R. Merletti, and H. Baare Olsen, "Evaluation of intra-muscular EMG signal decomposition algorithms," *J. of Electromyography and Kinesiology*, vol. 11, no. 3, pp. 175–187, Jun. 2001.
- [30] K. Akhmadeev, "EMG simulator for intramuscular multichannel and shifting electrodes," 2019, [Online repository](#).